



**FLUCOME 2009**

**10th International Conference on Fluid Control, Measurements, and Visualization  
August 17–21, 2009, Moscow, Russia**

## **GASDYNAMICS OF SLIDING AND DIELECTRIC BARRIER DISCHARGES IN AIR FLOW**

V.V. Volodin<sup>1</sup>, V.V. Golub<sup>2</sup>, A.S. Saveliev<sup>3</sup>

### **ABSTRACT**

The airflow around the airfoil with the heat release by the sliding discharge and dielectric barrier discharge (DBD) on its surface was studied in this work. The visualization of airflow around the airfoil with the electrical discharge and without it was performed. The spark sliding discharge on the conducting surface was initiated in one pulse or in frequency regime with frequency of 40 Hz and with the energy values from 1 to 100 J and with the voltage applied to discharger up to 5 kV. DBD was initiated in frequency regime with frequency of 60 kHz and with the power values from 50 to 100 W and with the voltage applied to discharger up to 5 kV. Two main diagnostic techniques were applied for flow visualization – the schlieren and the particle image velocimetry (PIV). In the case of electrical discharge the applying of PIV with smoke particles seeding is brought into question, because the particles can gain the charge portion in vicinity to the discharge area. Then under the electromagnetic influence they may diverge from the flow streamlines. This experimental work shows the possibility of PIV application with smoke seeding.

**Keywords: sliding discharge; dielectric barrier discharge; air flow**

### **INTRODUCTION**

Nowadays the aerodynamic control elements and the numerical models for calculation the aircraft trajectory control by the classical control were developed. But there are such regimes of aircraft flight that the usual control elements cannot function with enough efficiency, for example, when the angle of attack has the value that is close to critical angle (Kalugin, 2004). Under this conditions of aircraft flight the separation flows can appear and the redistribution of the pressure around the wing surface appears and thereby the controllability of the vehicle decreases, because the usually the control elements operates with maximum of the efficiency under the flow without a separation. In connection with this circumstances the attempts of using an active control elements, placed on the different parts of aircraft surface, which is functioning under nonaerodynamic principles, were taken. The first good results were achieved with using of the supersonic jet that was flowing outside from a slit at the supersonic airflow around the aircraft (Spaid & Zukoski, 1968). The distribution of the pressure on the surface, where the jet efflux was occurred, was measured and also the schlieren photographs of the jet and external supersonic airflow were obtained. The complex pattern of the spatial shocks, vortex and reverse flows interaction was

---

<sup>1</sup> Corresponding author: Joint Institute for High Temperatures, Russian Academy of Sciences, e-mail: [vlad@ihed.ras.ru](mailto:vlad@ihed.ras.ru)

<sup>2</sup> Joint Institute for High Temperatures, Russian Academy of Sciences

<sup>3</sup> Moscow Institute of Physics and Technology

reconstructed with the help of experimentally obtained photos.

In this work the spark sliding discharge on the conducting surface and dielectric barrier discharge (DBD) were used as nonaerodynamic active control elements. The discharges were initiated on the surface of the airfoil under the air flow for creating the additional drive force that can be used for changing the vehicle trajectory of flight. Simply the discharge influence on the air flow pattern around the model of wing can be imaging as shown on Fig. 1.

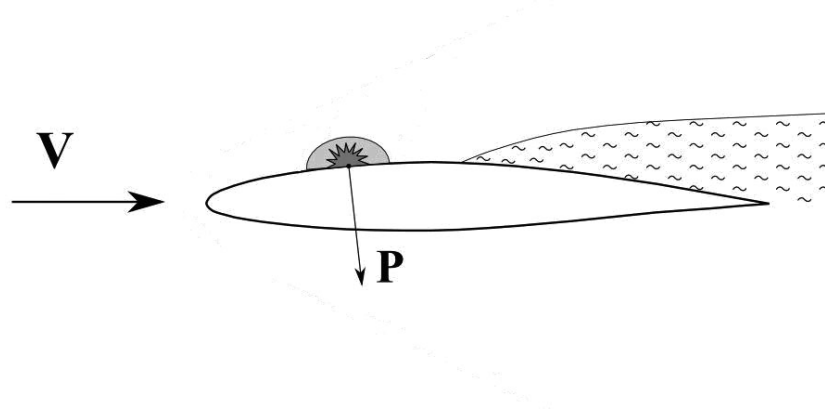


**Fig. 1. The discharge initiation in the air flow around the airfoil**

When the rapid local heat releasing appears the gas is heated up to several thousands of degrees of temperature value. Under these conditions at the point of discharge initiation the shock wave appears that leads to redistribution of static pressure on the surface of airfoil. With the sufficient shock wave intensity the laminar boundary layer can separate from the surface as the positive pressure gradient arises – the necessary condition for flow separation. Eventually the resultant force is acting on the upper surface of wing model during some period of time. If one take this time of force action into account, then one can say that the body in airflow gains some momentum that equals to force magnitude and time of action product.

The use of spark sliding discharge on the conducting surface is justified by following considerations. To initiate usual spark discharge in air it is necessary to apply the voltage between the electrodes that will provide the value of electrical strength equal to electrical strength breakdown of gas. This value usually is equal 30 MV/m for air at atmospheric pressure. To initiate spark discharge in the ten centimeters channel the voltage of 300 kV is needed to be applied between the electrodes. With use of spark sliding discharge on the conducting surface this value equals 2.5-5 kV on the ten centimeters distance between the electrodes and is in two orders less than in case of usual spark discharge. For the reason that the volume of gas involved into the sliding discharge is increased the portion of the energy that is releasing into air as a thermal energy is increased significantly comparing with the classical spark discharge (Aksenov *et al.*, 2007). Also it was shown that stable initiation of the sliding discharge on the conducting surface is possible in the subsonic and in supersonic gas flows.

Interest to DBD application in nonaerodynamic active control elements is caused by its relative simplicity of realization (2.5-5 kV voltage) and effectiveness in creation of flow disturbances, which may be used for aircraft control and for shift of flow separation conditions. DBD is the electrical discharge between two electrodes separated by an insulating dielectric barrier. Originally called silent discharge, and also known as ozone production discharge (Matsuno *et al.*, 1998), or partial discharge (Dhali &

Sardja, 1989), it was first reported by Ernst Werner von Siemens in 1857 (Siemens, 1857)

The process uses high voltage alternating current, often at lower RF frequencies but recently even at microwave levels. DBD devices can be made in many configurations, typically planar, using parallel plates separated by a dielectric, or cylindrical, using coaxial plates with a dielectric tube between them (Kraus *et al.*, 2001). In a common coaxial configuration, the dielectric is shaped in the same form as common fluorescent tubing, filled at atmospheric pressure with either a rare gas or rare gas-halide mix, with the glass walls acting as the dielectric barrier. Due to the atmospheric pressure level, such processes require high energy levels to sustain. Common dielectric materials include glass, quartz, ceramics and polymers. The gap distance between electrodes varies considerably, from 0.1 mm in plasma displays, 1 mm in ozone generators, or several cm in CO<sub>2</sub> lasers.

A multitude of random arcs form between the two electrodes during operation. As the charges collect on the surface of the dielectric, they discharge in microseconds, leading to their reformation elsewhere on the surface. Similar to other electrical discharge methods, the contained plasma is sustained if the continuous energy source provides the required degree of ionization, overcoming the recombination process leading to the extinction of the discharge. Such recombinations are directly proportional to the collisions between the molecules, and in turn to the pressure of the gas, as explained by Paschen's Law. The discharge process causes the emission of an energetic photon, the energy of which corresponds to the type of gas used to fill the discharge gap.

## EXPERIMENTAL SETUP

### Sliding discharge on the conducting surface

For the initiation of the sliding discharge on the conducting surface two designs of dischargers that are shown on the Fig. 2 a, b were developed.

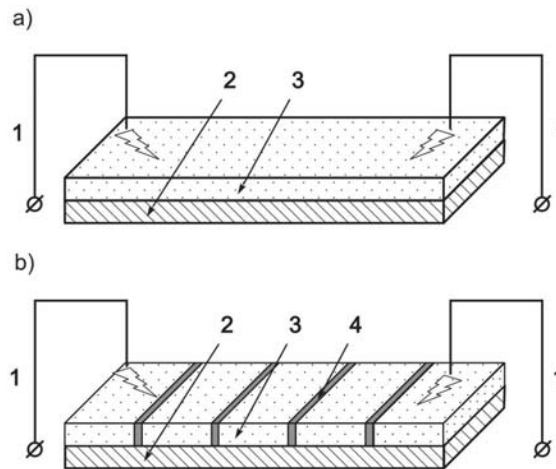


**Fig. 2. The usual (a) and the modified (b) scheme of the dischargers for spark sliding discharge initiation on the conducting surface. 1 – electrodes, 2 – dielectric plate , 3 – conducting surface, 4 – dielectric gap**

The common scheme of the discharger for initiation sliding discharge on the conducting surface is shown on the Fig. 2a. The conducting stripe (graphite) 3 of one decimeter in length and 5 mm in width is glued to the surface of the dielectric plate 2 (plexiglas or textolite). Near the ends of plate two electrodes

is mounted on the 1-2 mm distance from the conducting strip surface and the high voltage  $U$  is applied to electrodes. The electrical scheme of discharge power supplying is presented on the Fig. 3. The one single discharge energy is adjusted by varying of total capacity of a set of the capacitors  $C$ . The speed of capacitors charging and therefore the frequency of dischargers  $D$  functioning are regulated by varying the high voltage rheostat resistance  $R$ . After high voltage  $U$  applying the electrical breakdown of air gap between the electrodes and conducting surface. Then the initial streamers move in the direction to each other and form homogeneous plasma cord between the electrodes, where the electrical energy is releasing in thermal energy and in light emission. Due to the initial ionization of gas in air gap between the electrodes and conducting stripe the value of electrical strength breakdown decreases significantly.

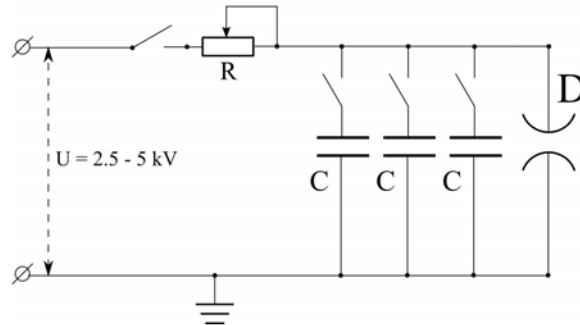


**Fig. 3. The electrical scheme for the discharge initiation.  $R$  – variable resistor,  $C$  – set of the capacitors,  $D$  – discharger**

It is known that the sliding discharge can finish by complete and incomplete stage of development. Incomplete stage is characterized by smaller discharge current and by smaller portion of electrical energy value that is releasing into the gas media. The residual electrical energy stored in the capacitors releases in the material of conducting stripe as intensive heating, what leads to continuous discharger's destruction. When the complete stage of discharge development is achieved the plasma cord shorts out the electrodes and the most intensive energy releasing occurs in gas medium. The experiments have shown that after the some value of the airflow velocity the development of sliding discharge in the moving gas ends on incomplete stage, because the air flow blows away the electrical arc and plasma cannot to short out the electrodes. In connection with this circumstance the modified scheme of discharger for sliding discharge initiation in air flows was developed, where the conducting surface is presented by segmented structure – the sequence of conducting segments of graphite and dielectric film of 0.15 mm thickness (Fig. 2b). The number of segments was varying from three to two tens in one discharger. The experiments have shown that using of the segmented conducting surface is more effective in subsonic and in supersonic airflow

### **DBD-plasma actuator**

On the Fig. 4 the sketch of discharger (or actuator) is presented. Usually the exposed electrode is a conducting tape, but in our case we have taken the highly conducting paint (that is used for rear window defogger repairing) to make very thin electrode. For the investigation DBD-discharge influence on the supersonic air flow ( $M = 2$ ) exposed electrode to be very thin to prevent flow separation or oblique shock appearance.

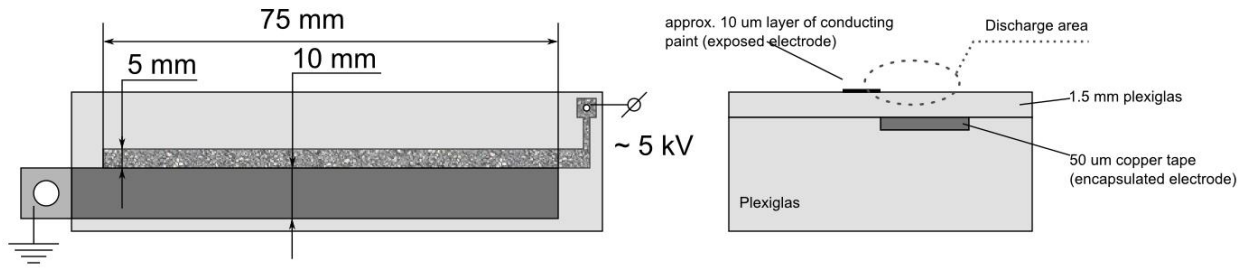


**Fig. 4. The sketch of the DBD-plasma actuator**

The high voltage AC power supply for this actuator has adjustable amplitude of voltage up to 5 kV, voltmeter and ampermeter for power consumption estimation. The operation frequency for this power supply is 60 kHz. On the Fig. 5 the oscillograms of the discharge current are presented with different time-scales. The measuring was carried out with noninductive shunt ( $R \sim 10^{-2}$  Ohm) and 100 MHz digital oscilloscope Tektronix TDS-3014B.

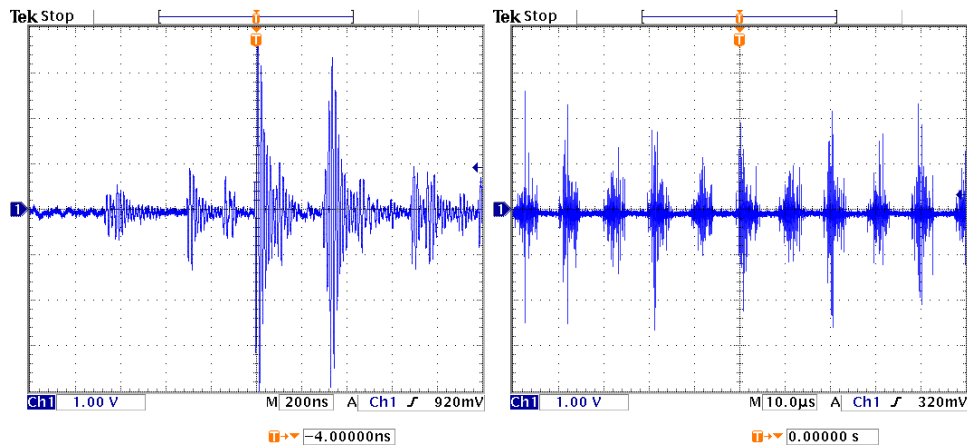


**Fig. 5. The typical oscillograms of DBD at 5 kV AC voltage amplitude and 60 kHz frequency**

### Supersonic wind tunnel

The process of airfoils streamlining by airflow was observed in the vacuum supersonic wind tunnel of periodical functioning with Mach number  $M = 2.0$  and with Reynolds number  $Re = 106$ . The maximum time of steady supersonic regime with Mach number  $M = 2.0$  equals 60 s. The mass rate of flow through the nozzle is about 1 kg/s. The scheme of the experimental setup is presented on Fig. 6.

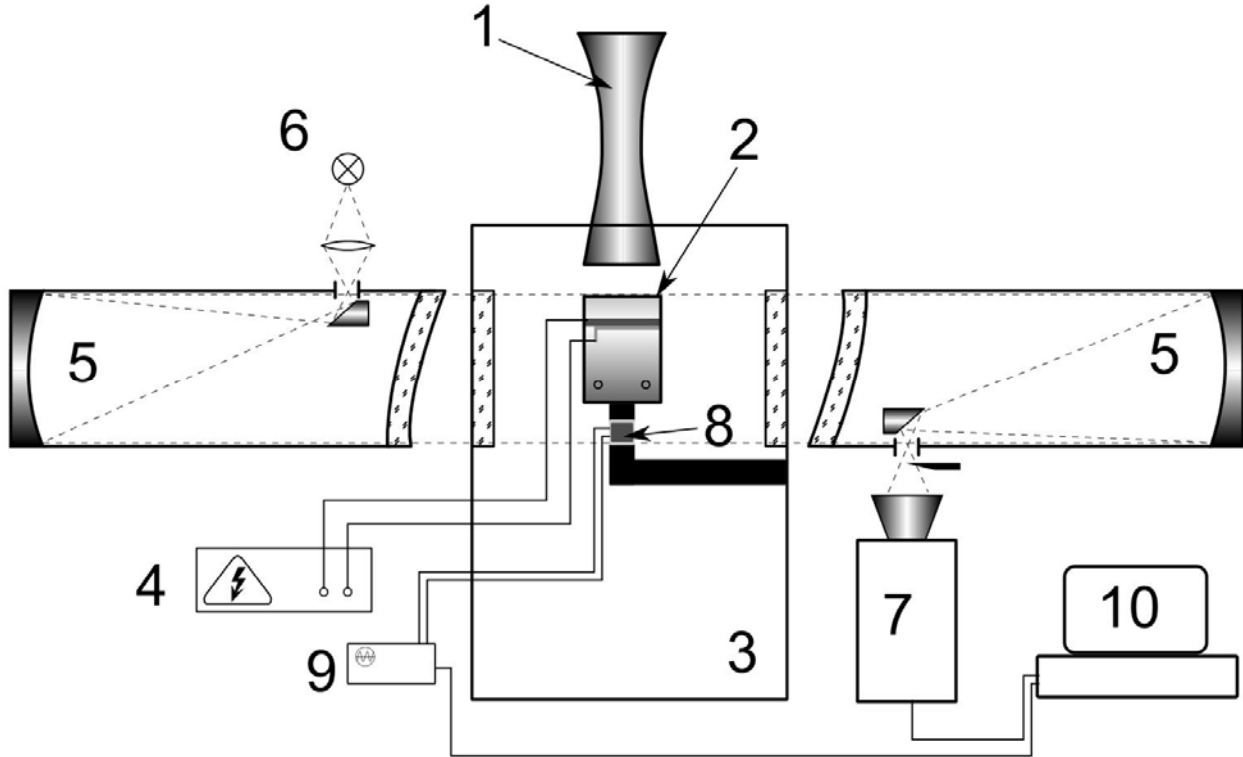


**Fig. 6. The supersonic vacuum wind tunnel of periodical functioning. 1 – nozzle, 2 – airfoil with discharger, 3 – working chamber with transparent windows, 4 – high voltage power supply, 5 – schlieren device IAB-451, 6 – lamp, 7 – CMOS videocamera Red Lake Motion Pro X3, 8 – strain sensor, 9 – ADC, 10 – computer**

Through the nozzle 1 the air is fills the preliminarily vacuumized working chamber 3 and connected to it gasholders with total volume of  $240 \text{ m}^3$ . Near the nozzle outlet the steady supersonic airflow forms with the velocity of  $520 \text{ m/s}$  and static pressure of  $0.12 \text{ atm}$ . In the flow the airfoil 2 with discharger, connected to electrical scheme (Fig. 3) and to high voltage power supply 4, is placed. Before the nozzle there is a receiver with lattices that reduce turbulent pulsations of airflow velocity value. The pressure in the gasholders and the static pressure in outer cross-section of nozzle (the diameter of this cross-section is  $110 \text{ mm}$ ) are measured with the vacuum gauges. The working chamber 3 has two windows of optical glass and the observation of airflow is leaded with the schlieren device 5 (IAB-451) that is made by the mirror-meniscus Maksutov's scheme. The visualization of supersonic airflow pattern around the airfoil has been performed by slit and knife method (Vasiliev, 1968). The lamp 6 was the  $50 \text{ W}$  incandescent lamp with the straight filament or filled with xenon capillary for the impulse illumination with the energy of one pulse  $5 \text{ J}$ . The optical device 5 for schlieren pictures of airflow around airfoil pattern obtaining is connected to high speed CMOS-videocamera 7 with speed of grab from 1 to 64 FPS and with minimum exposition time  $1 \text{ }\mu\text{s}$ . The data from videocamera 7 is collected by computer 8. The airfoil is made from dielectric material (textolite or plexiglas). In the upper surface of airfoil the discharger is mounted in such way that it is not disturbing the coming airflow. The airfoil is fastened with the aerodynamic support to rotation gear of working chamber. The support has strain sensor that can measure the force produced by airflow around the airfoil.

The air outflow through the de Laval nozzle into the working chamber is characterized by constant value of static pressure at outlet cross-section and by several regimes of functioning. The calculated static pressure at the nozzle outlet cross-section equals  $0.13 \text{ atm}$ . The minimum initial value of pressure in the

gasholders and working chamber is 0.01 atm. Therefore the air outflow is underexpanded and is characterized by presence of depression waves (Prandtl-Meyer's flow), that starts on the edge the nozzle. Going through the depression waves, the gas is continuously accelerated and the static pressure of flow is becoming equal to the pressure in working chamber. The underexpanded regime lasts for 40 s and is characterized by relatively weak airflow disturbance, thus such regime of air outflow is quite acceptable for supersonic airflow around the body research. The next and the relatively short-time (up to 5 seconds of duration) regime of airflow appears with the slow filling process of gasholders by air, when the pressure in the working chamber is become closer to the value of static pressure in the outlet nozzle's cross-section. Such regime of outflow («calculated» regime) is ideal for supersonic airflow around the bodies investigations, because in this case the jet doesn't «feel» any disturbances and freely outflows into the working chamber.

The next regime (overexpanded flow) of outflow appears when the pressure in working chamber increases up to value that is greater than the static pressure in the nozzle's outlet cross-section. In this case the oblique shocks that start on the edge of the nozzle appear in the jet and they match the static pressure in supersonic jet with the pressure in the working chamber. After several seconds the oblique shocks start to interact in irregular way, and the Mach's shock appears near the nozzle's outlet. With the gasholders filling by air the Mach's shock is going into the nozzle, disturbing the isentropic flow, and in the working chamber the supersonic flow is brought to stop. The overexpanded regime lasts for about 20 s. Schlieren visualization of airflow on the overexpanded regime indicates the very negative influence of shocks on the airflow without the flow separation and on the turbulence in total. The oblique shock wave, falling on the surface of airfoil, causes the untimely flow separation, and the Mach's shock, going into the nozzle, causes the flow separation on it's wall and strong turbulence of the subsonic airflow in working chamber. The investigation on this regime of airflow wasn't carried out, because the very intensive turbulence and a variety of shock's reflections on the working chamber's walls and airfoil's surface decrease significantly the quality of the schlieren photos. Though the values of the pressure in the gasholders exist, when it is possible to investigate the subsonic airflow in the working chamber with relatively weak turbulence of the jet. This period of the time is characterized by pressure incensement in the gasholders and working chamber, when the sonic speed of flow in de Laval nozzle's critical cross-section is not possible. The value of static pressure in the air jet is about 0.5 atm and the airflow speed is 200-250 m/s in this case (transonic).

## **RESULTS AND DISCUSSION**

### **Airfoil in the supersonic airflow**

The subsonic and supersonic airflow patterns around the airfoil are different. First of all, in the subsonic airflow the lift force is created by the air's rarefaction under the airfoil, but in the supersonic airflow this force is created by compression of gas in the area under the wing (Krasnov, 1971). This circumstance slightly moderates the negative influence of flow separation from the upper airfoil surface with the positive angles of attack. From the other side, the supersonic airflow around the airfoil is always characterized by the shock and oblique shocks. With the positive attack angles on the trailing edge in the supersonic airflow the oblique shock appears that matches the static pressure of airflow near the airfoil's surface with the ambient pressure (atmospheric pressure). The interaction of this oblique shock with the rather developed boundary layer causes the flow separation and pressure incensement near the trailing edge (Abramovich, 1991). As far as in this place the main control element of aircraft, the maneuverability of the vehicle decreases significantly.

On the Fig. 7 a, b the schlieren photos of the visualization of the airflow around the airfoil

NASA64A412 with the angles of attack 0 and 15 degrees correspondingly, obtained on the wing tunnel ST-4 with calculated regime of airflow, are presented. The airfoil is made from the plexiglas and it is 15 cm in width and it's chord length is 10 cm. Its surface is polish up to glance for the prevention of unwanted airflow disturbance.

The next difference of the conditions of streamlining between the subsonic and supersonic airflow is the presence of bow shock wave in the second case (supersonic).

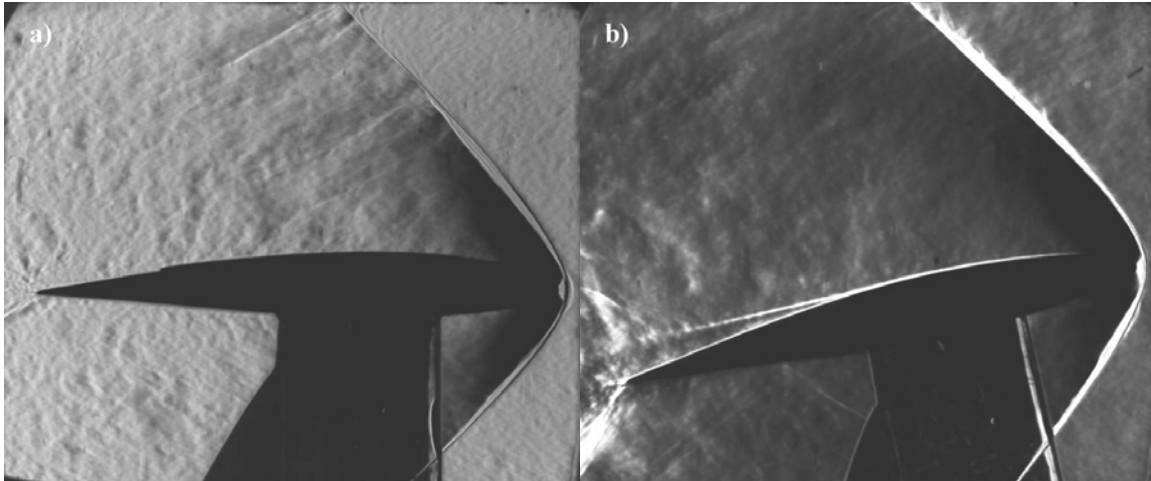


**Fig. 7. Supersonic airflow around the NASA airfoil under the 0 (a) and 15 (b) degrees of attack. The velocity of the airflow is 520 m/s (Mach number  $M = 2.0$ ). The schlieren photos is taken with the exposition of 2  $\mu$ s**

This circumstance is leading to the significant value of drag (shock-wave drag). In the case of real aircraft except the wings there are other elements of construction and the shocks can starts on them in the supersonic regime of flight. The interaction between these shocks and the boundary layer around the wing surface also impairs the aerodynamic characteristics, maneuverability and the stability of flight. The experiments (Chapman *et al.*, 1957) show that the location of separation point of the supersonic flow and the value of pressure incensement in stagnation region are in dependence on the Reynolds number. In the subsonic regime this effect cannot be observed (Chapman *et al.*, 1957). The Reynolds number can be varied by the increasing of flight altitude of aircraft or by the changing of flight speed.

### **Sliding discharge under the supersonic airflow**

The main advantages of using the sliding discharge on the conducting surface are:

- - the low value of electrical strength breakdown comparing with the spark discharge (the value of electrical strength breakdown is in two orders) and, as a consequence, the possibility for electrical discharge creation on the relatively huge distances between the electrodes;
- - the possibility of discharge initiation as in subsonic as well in the supersonic airflows;
- - wide range of energy release values, that are limited by maximum power of high voltage source and by the thermal load on the discharger, in the discharge;
- - wide range of values of ratio between electrical strength breakdown and the static pressure of gas  $E/p$ ;
- - the stability of discharge to the high humidity of the air flow (Aksenov *et al.*, 2009)[8].

Among all disadvantages of sliding discharge using as active control element of vehicle's trajectory

changing it is possible to mark the existence of the incomplete stage of discharge development, that is characterized by the high value of thermal energy release in the material of conducting surface, and therefore the thermal destruction of the discharger. First of all, this circumstance constrains the maximum value of the discharge frequency and the value of the electrical energy of single discharge initiation. In this work the stable initiation of sliding discharge with value of energy of 300 J was obtained. The maximum frequency was 40 Hz. On the Fig. 8 the schlieren photos of the sliding discharge initiation on the surface of airfoil in the quiescent air are presented. The discharger that is mounted in the wedge has 3 segments that are 2 cm in width each. The wedge is fastened in working chamber with the aerodynamic support with a strain sensor that allows measuring of the force of vertical direction. The first frame corresponds to quiescent atmosphere without discharge initiation. On the second frame the start of discharge and the leader creation in the gap between the electrodes and the conducting surface can be seen. The third frame shows the creating of plasma glow and of the products of discharger's material (graphite). The next frames show the relatively slow (comparing with the discharge initiation process) process of gas relaxation after the discharge initiation.

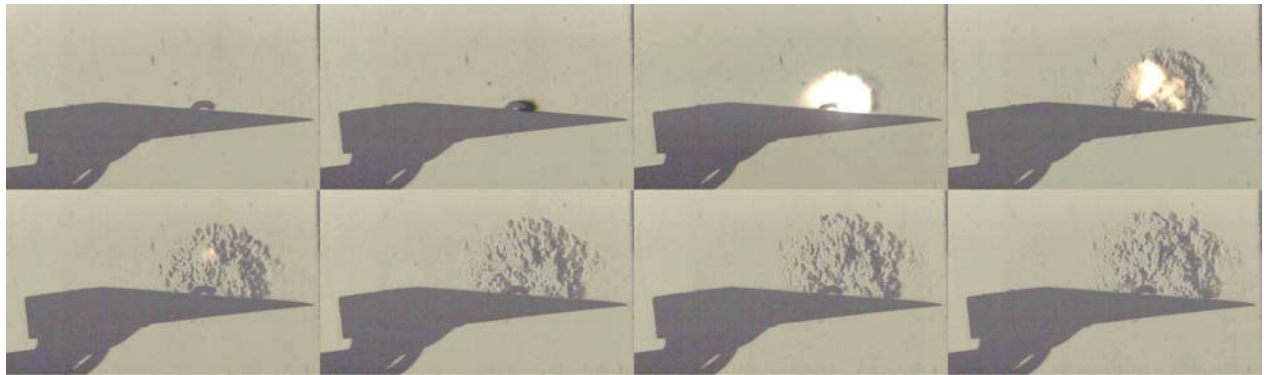


**Fig. 8. The schlieren photos of the discharge initiation process without the airflow. Sequenced frames (or photos) were taken every 500  $\mu$ s, the exposition time of each photo is 100  $\mu$ s**

The supersonic airflow changes the thermal load on the material of the conducting surface with the discharge initiation of the same value of electrical energy (30 J). On the schlieren photos (Fig. 9) the supersonic airflow pattern around the wedge with small positive angle of attack with the sliding discharge initiation can be seen. On the first frame the initial leader that has appeared between the electrodes and the conducting surface can be seen. Then the leaders met each other and the plasma cord appears with the thermal energy release in gas. On the third frame the last stage of discharge development is shown, when the plasma is significantly blown off by airflow, but the energy release continues by thermal and light emission. The small region of light emission is a electrical breakdown between the discharger and the support's element that is connected with the working chamber.



**Fig. 9. Development of the sliding discharge on the conducting surface in supersonic airflow. The exposition time of each photo is 100  $\mu$ s**

With the view of photo sequence it becomes clear that the airfoil vibrates under the supersonic airflow with the small value of amplitude. This fact is registered by the strain sensor of aerodynamic support. This circumstance is needed to take into account with the measuring of momentum that is produced by sliding discharge on the surface of airfoil

Initiation of sliding discharge causes the damped oscillations of airfoil. Strain gain of support registers these oscillations. On the Fig. 10 the oscillogram that corresponds to the case presented on the Fig. 8 is shown.

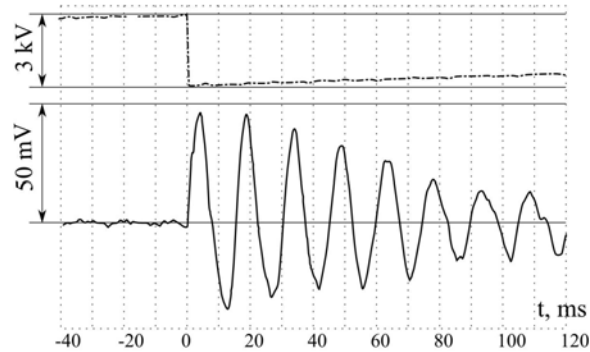


**Fig. 10. The oscillogram of the voltage applied to discharger (dotted curve) and of the strain sensor's signal (continuous curve)**

It is necessary to mark that under the airflow the airfoil is always slightly vibrates. Therefore with the energy release on the surface of streamlined airfoil the amplitude of these oscillations changes: it increases if the discharge is turned on in phase, and it decreases if the discharge initiation is in counterphase. On the Fig. 11 the typical oscillograms are shown, where the one corresponds to sinphase case, the second – counterphase and the third – the averaged signal of strain sensor that can be observed in the experiment.

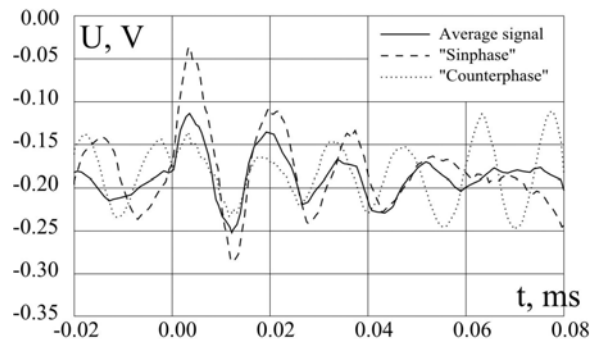


**Fig. 11. Typical oscillograms of the strain sensor's signal of the airfoil oscillations in the supersonic airflow**

On the Fig. 12 the oscillograms of oscillation for supersonic airflow and quiescent air cases are shown. It is clear that under the airflow the amplitude of oscillations is greater than in case of quiescent air, therefore the momentum created by sliding discharge is greater in case of moving air.

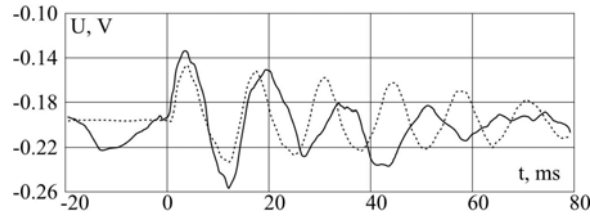


**Fig. 12. The oscillograms of the airfoil oscillations with sliding discharge initiation in the quiescent air (dotted curve) and in the supersonic (continuous curve) airflow 520 m/s**

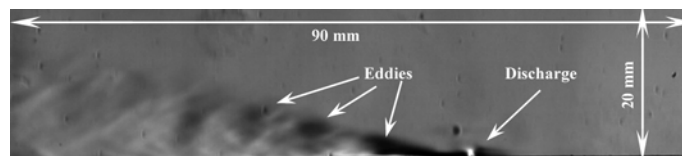
The calibration of strain sensor was made to measure momentum. Plasticine ball of mass 5 g falls on the discharger with airfoil from the height 1 m and sticking on it. Their collision can be taken as perfectly inelastic impact. In accordance with the conservation law the momentum, that airfoil gains after the collision, can be determine and measure it with strain sensor. Therefore, the amplitude of signal from the sensor can be precisely translated into momentum, which the airfoil gains after the impact or after discharge initiation on its surface.

The supplementary momentum, applied on streamlined airfoil after rapid heat releasing by sliding discharge, was measured. With the maximal electrical energy value of 250-300 J the supplementary momentum is about  $10^{-2}$  N·s.

It is reasonable to introduce the efficiency of supplementary drive force creation by siding discharge initiation. Under the efficiency of discharge we mean the ratio of supplementary momentum P and stored electrical energy E:  $\eta$  [s/m] = P[N·s]/E[J]. In the supersonic airflow the efficiency is about  $0.4 \cdot 10^{-4}$  s/m. For comparing, this efficiency for the modern firearms is about  $10^{-3}$  s/m, if we take the E as a thermal energy of powder combustion and the momentum P as a momentum of bullet  $P = m \cdot V$ . Therefore, the efficiency of creation of supplementary drive momentum by the electrical sliding discharge on the airfoil surface in supersonic airflow is only in one order less than the efficiency of modern firearms that is created for maximum momentum creation.

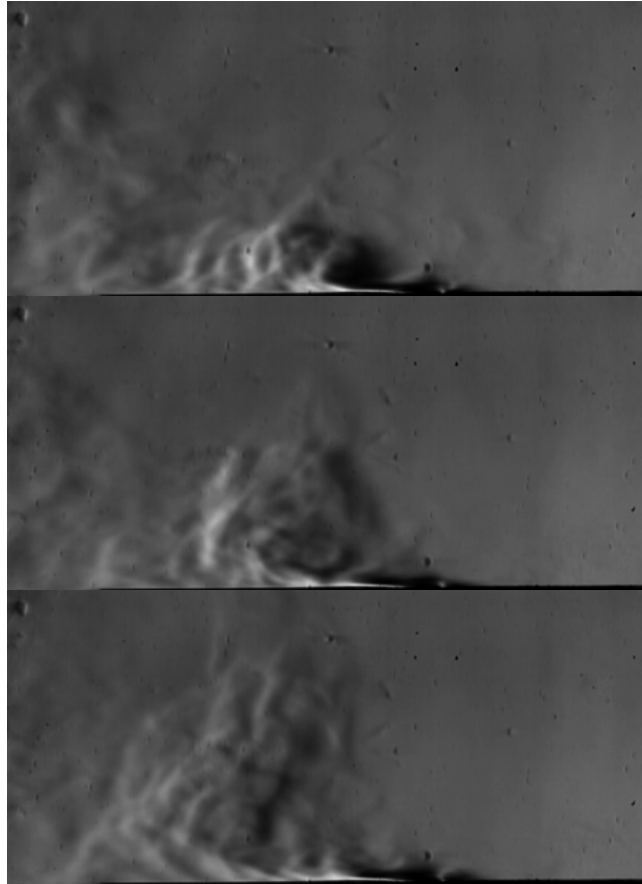
### Visualization and PIV-measurements of the wall jet produced by DBD

The 1000 FPS video acquisition was carried out and the velocity of wall jet, produced by DB-discharge, was measured in quiescent air at atmospheric pressure. The schlieren technique for velocity measurement was shown in (Sosa *et al.*, 2006; Opaitis *et al.*, 2007) and the main idea for measurement is to watch the eddies, that occur in turbulent discharge jet and can be considered as the tracers. These eddies appears in DB-discharge with AC power supplying. In our case the frequency of eddy creation is exactly 100 Hz, that is equal to doubled frequency of electricity network. On the Fig. 13 one frame of acquisition is presented. By the visible eddies the wall jet velocity can be determined. The measured by schlieren high speed video registration jet velocity is 1 m/s.



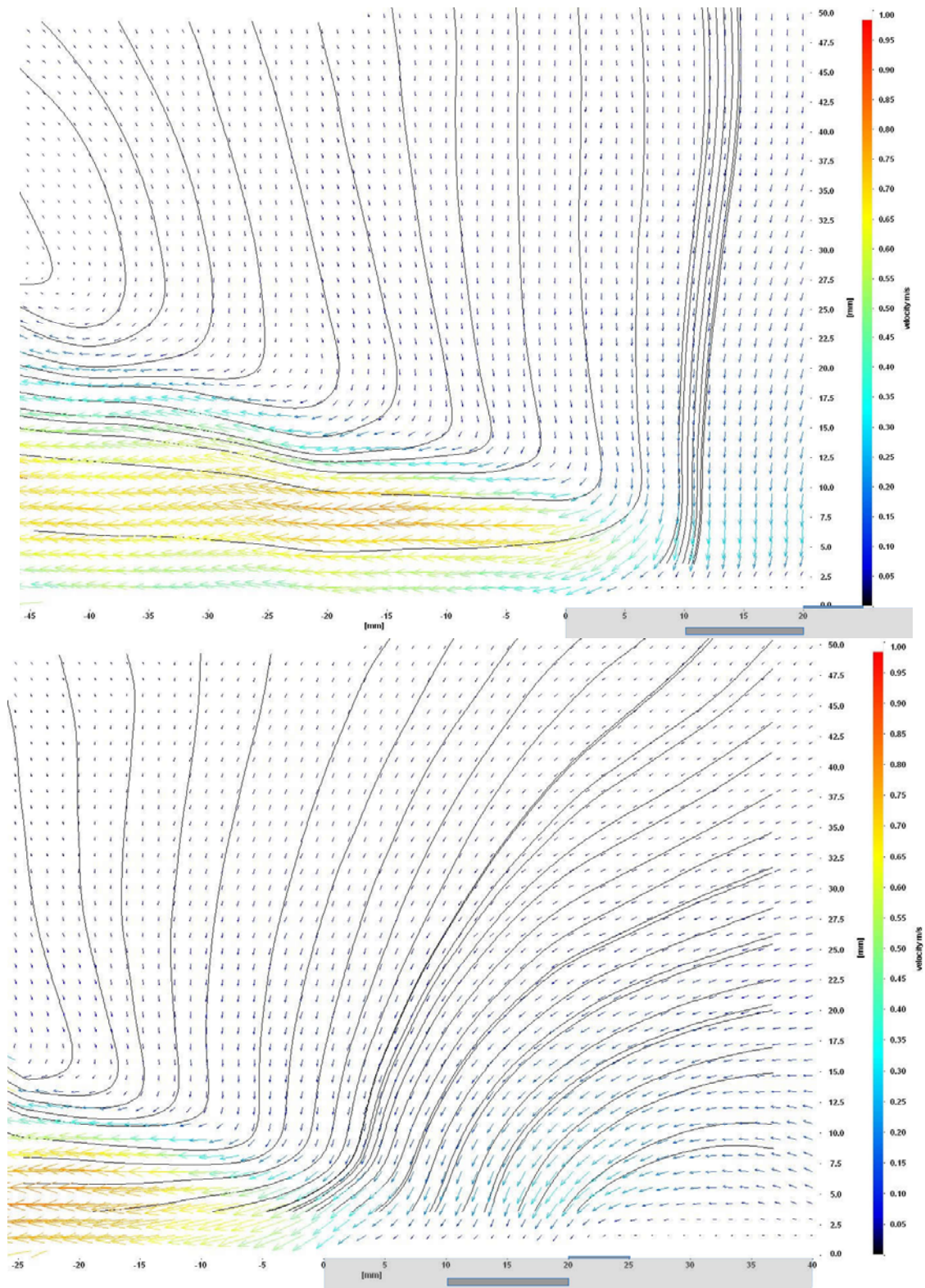
**Fig. 13. Schlieren frame from 1000 FPS video acquisition at 1 atm of initial pressure. Time exposition = 700 μs**

Fig. 14 shows clockwise vortex creation and its propagation from right to left side of picture. In other words, the vortex drifts with the wall jet, created by DBD. The visible vortex diameter increases up to 30 mm.



**Fig. 14. Schlieren frame sequence from 1000 FPS video acquisition at 0.5 atm of initial pressure. Time exposition = 700  $\mu$ s, frame time spacing 10 ms**

The next step was the determination of possibility of the real tracers using like smoke particles without significant error in jet velocity magnitude. We have used LaVision PIV Flow Master 3 with 2 MP (1600x1200) ICCD camera and double head LitronLasers Nano L 125-15 PIV laser Nd:YAG 532 nm. The camera was equipped with the 532 nm filter to reduce the background light in second frame in double frame regime. The visible area was 50x50 mm, the interrogation window is 64 px and the max velocity 1 m/s. This information leads to  $dt = 270 \mu$ s between two frame. The acquisition consists of 20 doubleframes and with 14 Hz frequency. The seeding was the smoke that is produced by organic material combustion (particles of approx. 1  $\mu$ m in diameter). On the Fig. 15 two PIV-measurements that are corresponding different position of discharger are presented. On the left picture the wall jet velocity distribution is presented, but on the right picture the flow in front of the discharger can be seen. On these picture averaged by all 20 frames in acquisition 2D velocity vector field and streamlines are shown. On the Fig. 16 the one frame from PIV processed acquisition is shown with eddy that was visible in schlieren pictures too. One can see that PIV ( $V_{jet} = 1.0$  m/s) and schlieren ( $V_{jet} = 1.0$  m/s) techniques for velocity measurement are in good correspondence.



**Fig. 15. Time-averaged by 20 frames (14 FPS double-frame acquisition) vector field**

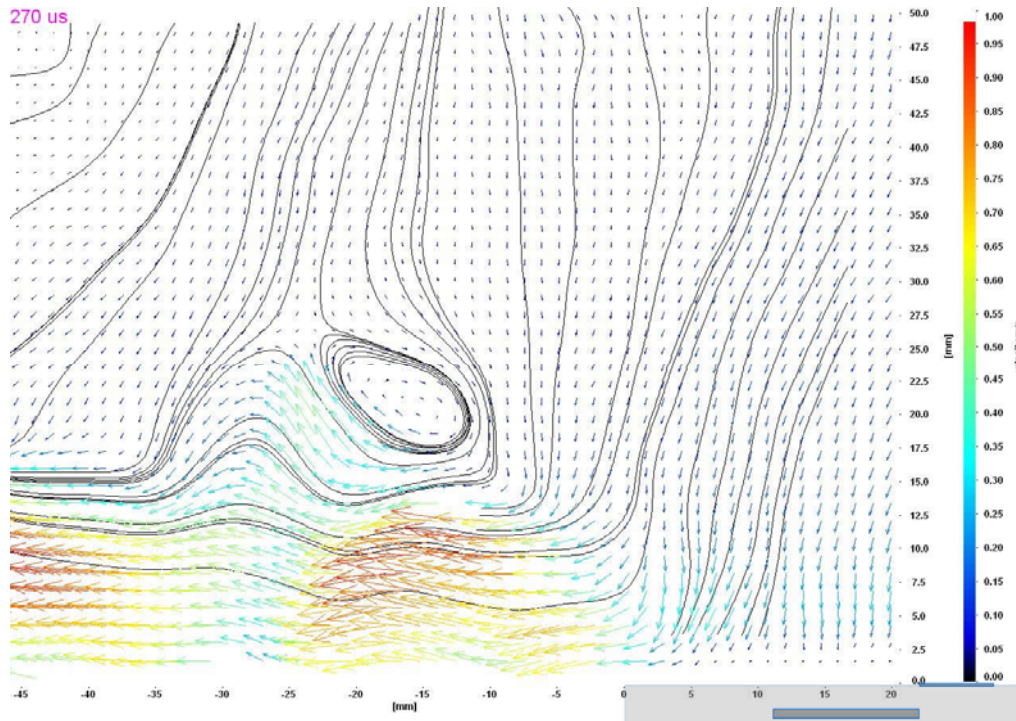


**Fig. 16. Example of processed double-frame in acquisition**

## SUMMARY

Experiments on the initiation of high- and low- temperature plasma by ark sliding and DB discharges correspondingly in the airflow with Mach number  $\leq 2$  are carried out.

The main parameters that affects on sliding discharge on conducting surface are defined and the conditions, under which the initiation of discharge is possible in frequency regime in subsonic and supersonic airflow, are obtained. It appears, that the main condition for sliding discharge initiation is a value of the electrical field strength, because with certain voltage the airflow speed cannot affect on the process of discharge creating. The static pressure in flow also can affect on process of initiation of discharge, because it define the breakdown electric strength of air. The frequency of discharge initiation is also has matter as too frequent thermal energy releasing results in overheating and destruction of conducting material. The possibility of using the pulse-periodic heat releasing on the surface of aircraft for creating supplementary drive force is experimentally shown. The ability to initiate sliding discharge in frequency mode up to 40 Hz is shown. The additional momentum, created by sliding discharge initiation on the surface streamed by subsonic and supersonic airflow, is measured. The efficiency of creating supplementary drive force by discharge is estimated.

The asymmetric DBD was obtained in supersonic airflow with the Much number  $M = 2$  and with the static pressure in jet  $p = 0.15$  atm. The influence of static pressure value on the form and regime (filamentary or homogeneous plasma layer) of DBD is estimated. It was found that the high-speed airflow significantly affects on the width and thickness of plasma layer. The discharge current were measured and the applied power was registered. The high-speed schlieren videoregistration of DBD development that allows measuring the wall jet velocity was obtained. Also the spatial velocity distribution of the wall jet was obtained by 2D planar PIV system. The experiment has shown that the values of velocities measured with the schlieren velocimetry and PIV, based on particle seeding, are in good correspondence. Thereby,

in work the possibility of DBD plasma actuator using in supersonic airflow is shown and the investigation of static pressure and airflow velocity influence on the form and regime of dielectric discharge development was performed.

## ACKNOWLEDGMENTS

The investigation was partially supported by Presidium of Russian Academy of Sciences Program #11.

## REFERENCES

- Abramovich, G.N. (1991), "Applied gasdynamics, part 2," Nauka, Moscow.
- Aksenov, V.S., V.V. Golub, S.A. Gubin, K.V. Efremov, I.N. Laskin and V.V. Volodin (2007), "Experimental and numerical investigation of impulse created by sliding electric arc discharge on semi conducting surface in the subsonic and supersonic flows," proceedings of European conference for aero-space science, Brussels, Belgium, 2007) Paper 5-06-05.
- Aksenov, V.S., V.V. Golub, S.A. Gubin, A.S. Saveliev, V.A. Sechenov and E.E. Son (2009), "Sliding Discharge Control for Aircraft," AIAA 2009-696 47th AIAA Aerospace Sciences Meeting including The New Horizons Forum and Aerospace Exposition, Orlando, Florida, Jan. 5-8.
- Chapman, D.R., D.M. Kuchn and H.K. Larson (1957), "Investigation of Separation Flows in Supersonic and Subsonic Streams with Emphasis on Effect of Transition," NASA TN 3869.
- Dhali, S.K. and I. Sardja (1989), "Dielectric-barrier discharge for the removal of SO<sub>2</sub> from flue gas," IEEE International Conference on Plasma Science, IEEE Conference Record - Abstracts.
- Kalugin, V.T. (2004), "Aerodynamics of control elements of aircraft flight," MSTU n.a. N.E. Bauman, Moscow.
- Krasnov, H.F. (1971), "Aerodynamics," High School, Moscow.
- Kraus, M., B. Eliasson, U. Kogelschatz and A. Wokauna (2001), "CO<sub>2</sub> reforming of methane by the combination of dielectric-barrier discharges and catalysis," Physical Chemistry Chemical Physics, **3**, 294-300.
- Matsuno, H., N. Hishinuma, K. Hirose, K. Kasagi, F. Takemoto, Y. Aiura and T. Igarashi (1998), "Dielectric barrier discharge lamp," United States Patent 5757132
- Opaits, D., G. Neretti, A. Likhanskii, S. Zaidi, M. Schneidern R. Miles, S. Macheret. (2007), "Experimental investigation of DBD plasma actuators driven by repetitive high voltage nanosecond pulses with DC or low-frequency sinusoidal bias," AIAA-2007-4532, 38th AIAA Plasmadynamics and Lasers Conference, Miami, FL.
- Siemens, W. (1857), "Ueber die elektrostatische Induction und die Verzögerung des Stroms in Flaschendräten," Poggendorffs Ann. Phys, Chem **102**, 66-120.
- Sosa, R., E. Arnaud, G. Artana (2006), "Schlieren Image Velocimetry applied to EHD flows," International Symposium on Electrohydrodynamics (ISEHD), Buenos Aires, Argentina.
- Spaid, F.W. and E.E. Zukoski (1968), "A study of the interaction of gaseous jets from transverse slots with supersonic external flows," AIAA Journal, 0001-1452, vol.6, no.2, 205-212p.
- Vasiliev, L.A. (1968), "Schlieren methods," Nauka, Moscow.